Optical Materials 102 (2020) 109830

Contents lists available at ScienceDirect

Optical Materials

journal homepage: http://www.elsevier.com/locate/optmat

Bismuthene quantum dots based optical modulator for MIR lasers at 2 μm

Han Pan [a,1], Weichun Huang [b,1], Hongwei Chu [a,**], Ying Li [c], Shengzhi Zhao [a], Guiqiu Li [a], Han Zhang [a,d], Dechun Li [a,*]

[a] School of Information Science and Engineering, Shandong University, Qingdao, Shandong, 266237, China
[b] College of Chemistry and Chemical Engineering, Nantong University, Nantong, 226019, China
[c] Key Laboratory of Colloid and Interface Chemistry of Education Ministry, School of Chemistry and Chemical Engineering, Shandong University, Jinan, Shandong, 250100, China
[d] Collaborative Innovation Center for Optoelectronic Science & Technology, International Collaborative Laboratory of 2D Materials for Optoelectronics Science and Technology of Ministry of Education, College of Physics and Optoelectronic Engineering, Shenzhen University, Shenzhen, 518060, China

ARTICLE INFO

Keywords:
Bismuthene quantum dots
Nonlinear optical properties
Open-aperture Z-scan
Saturable absorber
Q-switching lasers

ABSTRACT

The uniformly sized two-dimensional (2D) bismuthene quantum dots (BiQDs) were fabricated through the liquid-phase exfoliation (LPE) route and characterized comprehensively. By transferring the BiQDs onto a quartz substrate, BiQDs saturable absorber (SA) was prepared and applied in a Tm:YLF bulk laser. To get the best output performance of passive Q-switching (PQS) laser with BiQDs-SA, three output couplers with different transmittance were applied in laser implementation. The stable solid-state 2 μm laser was obtained, generating a maximum peak power of 8.1 W and shortest pulse width of 440 ns with the T = 5% output coupler. To the best of our knowledge, it is the first demonstration of BiQDs-SA for Q-switching operation around 2 μm, implying that the BiQDs-SA can be considered as a promising optical modulator for the mid-infrared (MIR) pulses producing.

1. Introduction

In recent decades, the pulsed lasers in the mid-infrared (MIR) region, especially around 2 μm, have drawn a plenty of attention due to the potential application prospects in numerous fields (such as medicine treatment, materials processing, free-space communication, and detection) [1–4]. Additionally, the pulsed laser emitting the radiation around 2 μm is an effective approach of driving MIR optical parametric oscillators (OPOs) [2]. Basically, Q-switching is usually employed to generate pulsed laser via active or passive techniques. Up to date, extensive Q-switching operations in thus MIR regime have been demonstrated in terms of solid-state and fiber lasers. Among them, the thulium (Tm^{3+}) ion is extremely attractive for emitting lasers in this region because of its wavelength emission at ~2 μm ($^3F_4 \rightarrow {}^3H_6$ transition). Therefore, Q-switched all-solid-state 2 μm lasers based on Tm-doped gain medium have been reported [5–7]. Compared with the complicated and bulky active Q-switching technique, passive Q-switching (PQS) technique is one more efficient means to obtain pulsed lasers, possessing some obvious advantages for instance compact, easily-operated and low-cost [8].

For the PQS operation, the most critical component is the saturable absorber (SA). For the last few decades, numerous novel SAs have been utilized in lasers operating around 2 μm wavelength, including carbon group materials like graphene [9], single-walled carbon nanotubes (SWCNTs) [10], and other layered two-dimensional (2D) nanomaterials for instance transition metal chalcogenides (TMDs) [11], black phosphorus (BP) [12], and topological insulators (TIs) [13]. Although the 2D materials have the advantages of being readily available, the amorphous morphology and hundreds-nanometers sizes usually lead to poor uniformity [11–13], which makes the pulse unstable. In addition to the 2D materials, quasi zero-dimension quantum dot (QD) with size of several nanometers exhibits excellent optoelectronic properties due to the quantum confinement effect and size-edge effect [14]. So far, researchers have fabricated carbon and MoS_2 QDs and employed them in photovoltaic devices [15], optoelectronics [16], and biological analysis [17,18]. The impressive results stimulated researchers to make more effort to explore QDs family members.

On the other hand, the Group-VA monolayers arouse much interest

* Corresponding author.
** Corresponding author.
E-mail addresses: hongwei.chu@sdu.edu.cn (H. Chu), dechun@sdu.edu.cn (D. Li).
[1] These authors contributed equally to this work.

https://doi.org/10.1016/j.optmat.2020.109830
Received 15 January 2020; Received in revised form 26 February 2020; Accepted 10 March 2020
Available online 18 March 2020

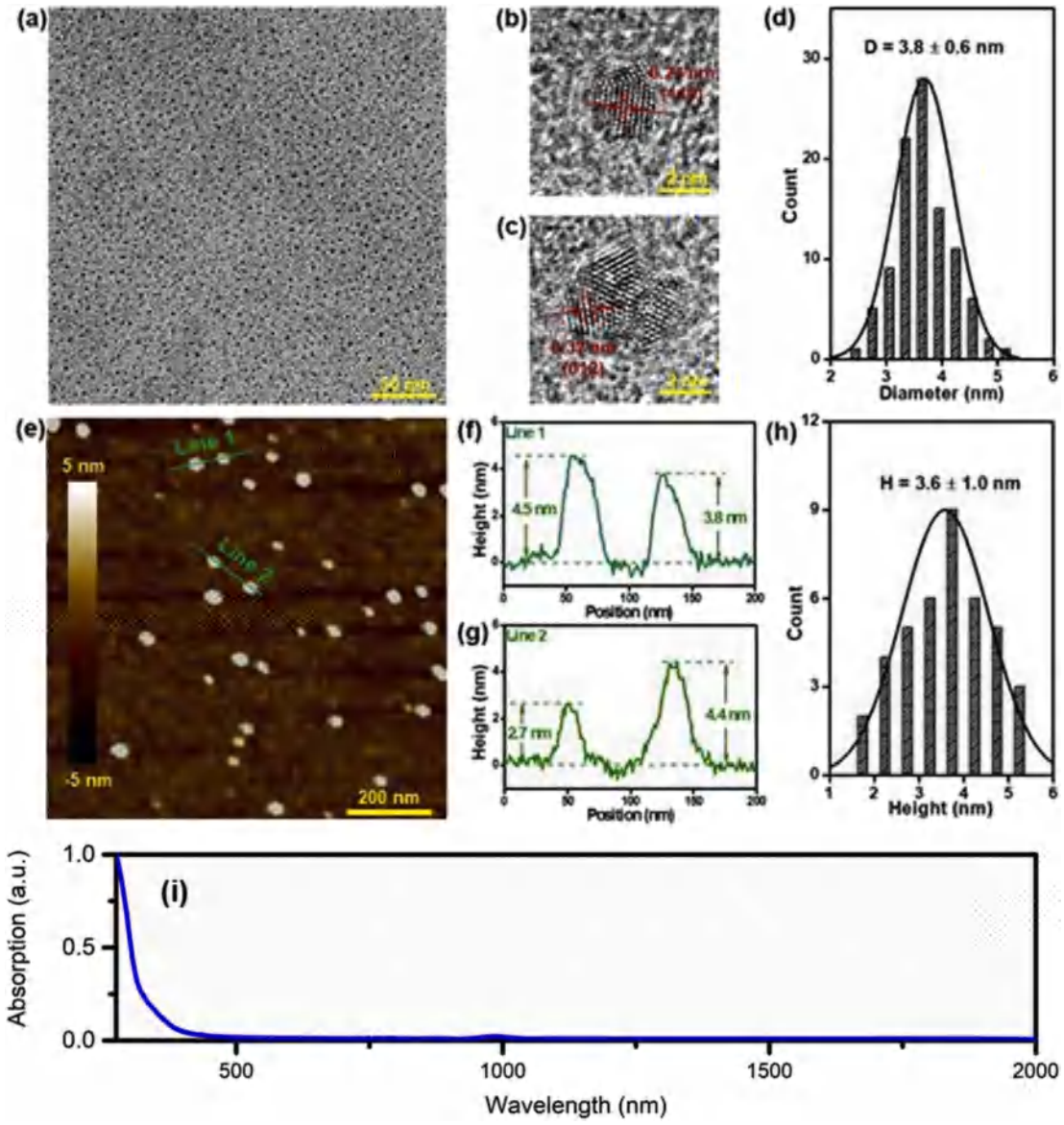

Fig. 1. The morphological and structural feature of as-prepared BiQDs. (a) TEM image. (b, c) HRTEM images with different lattice fringes. (d) Statistical analysis of the size based on an amount of about 100 BiQDs captured in the TEM image. (e) AFM image. (f, g) Height profiles along the green lines in (e). (h) Statistical analysis of the heights based on approximately 40 BiQDs measured by AFM. (i) The linear absorption spectra of the BiQDs sample range from 270 nm to 2000 nm. (For interpretation of the references to colour in this figure legend, the reader is referred to the Web version of this article.)

due to their broadband absorption property, which caused by wide range of band gaps from 0.36 to 2.62 eV. As the most concerned Group-VA 2D material, black phosphorus (BP) has been indicated to possess excellent nonlinear optical (NLO) properties and employed as SA in bulk laser generation [13]. Recently, Xu et al. synthesized BP quantum dots (BPQDs) and investigated their NLO properties [19]. However, the development of BP-based applications was limited by the inherent instability and susceptibility to oxidation in ambient condition [20–22]. Therefore, researchers not only focus on solving the issues of oxidation and long-term stability [23,24], but also continuously develop new Group-VA 2D materials with excellent optoelectronic property and good chemical stability [25]. Unlike BP, another Group-VA material, bismuth (Bi), is typical semimetal in a layered bulk state of nature [26], which possesses higher chemical stability than BP in normal condition. Based on first-principle calculations [26–28], it is also theoretically predicted to possess enhanced stability and unique properties. In this case, with considering the high scalability, Bi has attracted more attention among monoelemental 2D nanomaterials. Inspired by the unique feature of graphene and TMDs QDs, as well as the novel chemical and physical properties of bismuth materials, we synthesized high quality BiQDs for the NLO research.

In this work, uniform-sized BiQDs (approximately 4 nm) were prepared by the liquid-phase exfoliation (LPE) route. The NLO properties of BiQDs were investigated by the Z-scan technique. Owing to the saturable absorption feature, the BiQDs were successfully applied in 2 μm solid-state pulse laser as an optical modulator. A passive Q-switching (PQS) Tm:YLF laser was presented with employing BiQDs as the SAs for the first time. The stable PQS laser pulse with the minimum pulse width of 440 ns at the repetition rate of 93.6 kHz are realized with T = 5% OC, corresponding to the single-pulse energy of 3.6 μJ and the peak power of 8.1 W. The demonstration of BiQDs-SA based PQS laser operating around 2 μm region may promote the development of high-quality 2D monoelemental QDs in optical modulation field. In addition, it is also very meaningful for broadening the research path of 2 μm solid-state lasers.

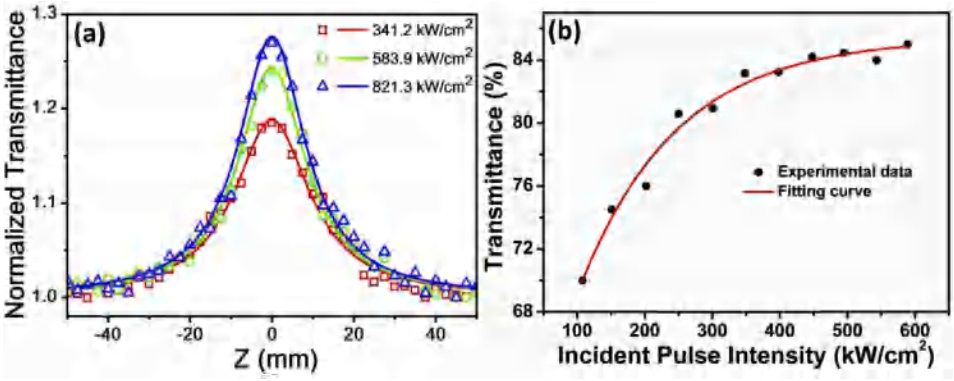

Fig. 2. NLO properties of the BiQDs-SA at 2 μm. (a) OA Z-scan results with different pump intensities (the inset data show the maximum intensity at z = 0). (b) NLO transmittance measurement results.

2. Experimental sections

2.1. Synthetic methods

Firstly, the original Bi powder was dissolved in N-methyl pyrrolidone (NMP) solution with a concentration of 5 mg/mL. Then the mixed solution was bath sonicated for 48 h with applying a power of 400 W. The work temperature was kept at 5 C by the built-in cooling water system during the whole process. Subsequently, the above mixture was filtrated through a porous anodized aluminum oxide (AAO) membrane, whose pore diameter is 100 nm, to eliminate large-sized Bi particles and then filtered again through an AAO membrane with a 20 nm pore diameter to obtain the BiQDs/NMP shallow dispersion. Ultracentrifugation with a speed of 18,000 rpm was carried out to the BiQDs/NMP dispersion for 25 min and the obtained precipitate was dehydrated in a vacuum oven for 24 h at 80 C.

2.2. Fabrication of BiQDs SA

The obtained BiQDs precipitate dispersed in NMP solution was sonicated, and then the supernatant was dropped carefully onto a quartz substrate, spread evenly, and finally dried in an oven with the constant temperature of 65 C for 12 h.

2.3. Characterization

The high resolution transmission electron microscopy (HRTEM) images were captured by a Philips Tecnai 20U-Twin HRTEM at an acceleration voltage of 200 kV. Digital Instruments Dimension 3100 AFM was utilized to explore the topographic morphology. A UV-VIS-NIR spectrophotometer (Hitachi U-4100) was used to obtain the linear absorption of the prepared BiQDs sample.

3. Results and discussion

3.1. Characterization and discussion

The morphological and structural characterizations of as-prepared BiQDs were shown in Fig. 1. TEM and HRTEM were utilized to observe the morphology of BiQDs. From the TEM images in Fig. 1(a), the average diameter of as-prepared BiQDs was counted as 3.8 ± 0.6 nm (Fig. 1(d)). The HRTEM images of BiQDs show lattice spacing of 0.21 nm (shown in Fig. 1(b)) and 0.32 nm (shown in Fig. 1(c)), corresponding to the (110) and (012) planes of the Bi crystal, respectively. The topographic morphology of BiQDs was characterized by atomic force microscope (AFM) (see Fig. 1(e)). Given that the average inter-atomic distance of one layer in bulk Bi is about 0.34 nm, the measured thickness of 4.5, 3.8, 2.7, and 4.4 nm (Fig. 1(f and g)) were corresponding to BiQDs with about 13, 11, 8 and 13 layers, respectively. The average thickness obtained by statistical AFM analysis was 3.6 ± 1.0 nm (Fig. 1(h)), corresponding to about 11 ± 2 layers. The linear absorption spectra ranging from 270 nm to 2000 nm were measured by a UV-VIS-IR spectrometer. In Fig. 1(i), it shows clearly that the as-prepared BiQDs sample undergoes a long process of the monotonically decrease from the ultraviolet to the mid-infrared regions.

The NLO properties of BiQDs-SA were investigated by the open-aperture (OA) Z-scan technique. The laser source was a home-made acousto-optic modulator (AOM) PQS laser emitting the pulses at 2 μm. As shown in Fig. 2(a), the Z-scan experimental results with different pump laser intensities were obtained. The experimental data were analyzed by the fitting equation as follows [29]:

$$T = \sum_{m=0}^{\infty} \frac{[-q_0(z,0)]}{(m+1)^{1.5}}, \quad m \in N \qquad q_0(z,0) = \frac{\beta_{eff} L_{eff} I_0}{(1+z^2/z_0^2)} \tag{1}$$

where $L_{eff} = (1 - e^{L\alpha_0})/\alpha_0$ represents the effective length, α_0 is the linear absorption coefficient, I_0 represents the on-axis peak intensity, L and β_{eff} represent the sample length and the effective nonlinear absorption coefficient, respectively.

From Fig. 2(a), it can be seen that the nonlinear absorption phenomenon is obviously observed at each pump intensity, that is, the transmittance increases nonlinearly with the augment of illuminating laser pump intensity (the sample was moved toward Z = 0). All normalized transmission curves show a symmetrical peak with respect to the focus (z = 0), implying that the nonlinear saturable absorption dominates the nonlinear process. In addition, it can be also concluded that the NLO response of BiQDs enhanced with the increasing pump intensities. The OA Z-scan results indicated that BiQDs have a strong optical switch capability at 2 μm band and is promised in optical modulator applications. To further investigate the NLO property of BiQDs at 2 μm, the simple NLO transmission measurement has also been presented. The laser source emitted laser pulses with the width of 70 ns and a repetition rate of 5 kHz. As shown in Fig. 2(b), the measurement data were fitted by the following equation [29],

$$T = 1 - \Delta T \exp(-I/I_S) - T_{ns} \tag{2}$$

Here, ΔT is the modulation depth, I_s is the saturable intensity and T_{ns} represents nonsaturable losses. The linear transmission of the BiQDs at 2 μm was determined as 69.4%. According to the fitting results, the modulation depth, saturation intensity and nonsaturable loss were determined as 15.4%, 183.9 kW/cm^2 and 14.9%, respectively. The nonlinear absorption characteristics indicated that the as-prepared BiQDs could be a potential optical modulator at 2 μm wavelength.

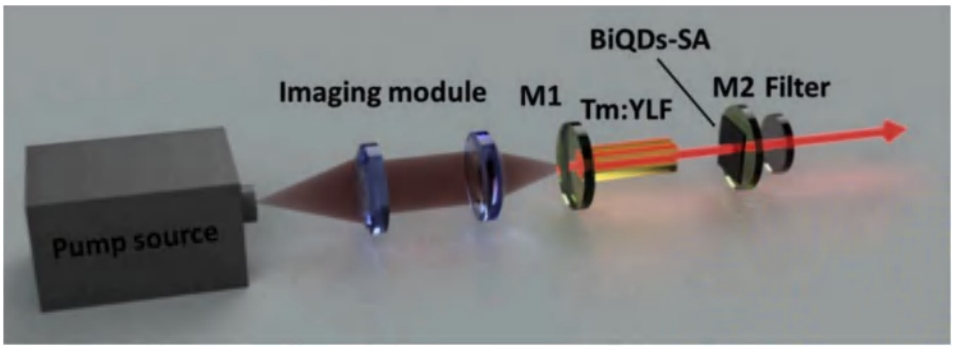

Fig. 3. Schematic of laser experiment setup.

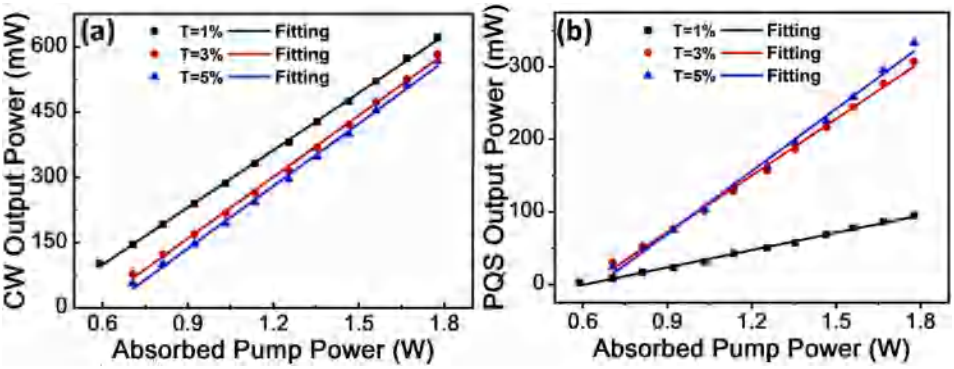

Fig. 4. AOP versus absorbed pump powers for the BiQDs-SA based Q-switched Tm:YLF laser. Dots represent measurement data and curves represent the linear fitting. (a) In CW and (b) Q-switching regime.

3.2. Laser experiment and results

To further investigate the practical saturable absorption property of BiQDs-SA, a PQS Tm:YLF laser with diode pumped was demonstrated (Fig. 3). The laser cavity was 1.5 cm long. A 794 nm fiber coupled diode laser was used as the pump source. The numerical aperture (NA) and

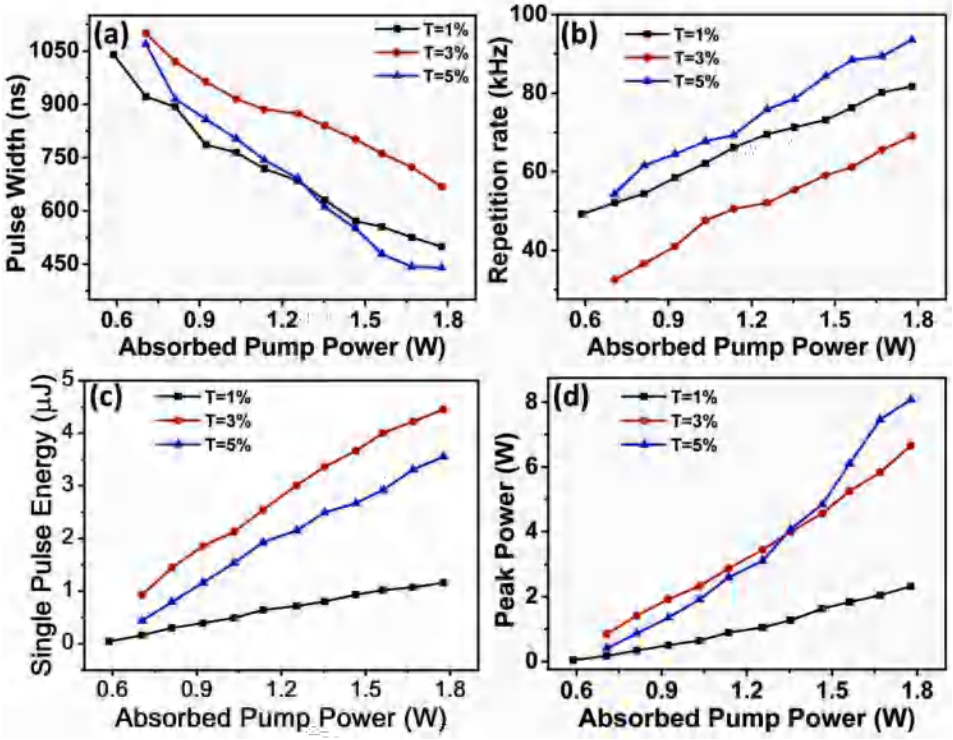

Fig. 5. The output performance versus absorbed pump powers from Tm:YLF PQS lasers.

diameter of the coupling fiber core are 0.22 and 200 μm, respectively. The pump laser beam was focused into the gain medium by a 1:1 imaging module. The input mirror M1 is a concave dichroic mirror with a radius of curvature of 200. Its surface is anti-reflectivity (AR) coated from 750 nm to 850 nm (R < 2%) and high-reflectivity (HR) coated from 1850 nm to 2100 nm (R > 99.9%). The flat mirror M2 is utilized as the output coupler (OC). To investigate the laser output characteristic, three OCs with the transmittance of 1%, 3% and 5% from 1820 nm to 2100 nm were utilized. The laser gain crystal is a 3 at.% doped Tm:YLF crystal (3 × 3 × 10 mm^3). To effectively reduce the thermal effect, the gain medium was wrapped with a thin indium foil and then embedded in a brass heat sink, which was maintained at 17 C by semiconductor and wind cooling. The SA was placed closely to the output coupler (OC) to saturate it by the beam waist formed in this cavity. The pulse temporal behavior was detected by a InGaAs biased photodetector (DET08 C/M, THORLABS Inc., USA) and recorded by a DPO 7104C digital phosphor oscilloscope (Tektronix Inc., USA). A power meter (MAX 500AD, Coherent Inc., USA) was employed to evaluate the average output power (AOP).

The continuous wave (CW) Tm:YLF laser characteristic were recorded firstly. As displayed in Fig. 4(a), all sets of AOP with different transmittances OCs are increased almost linearly. At 1.8 W absorbed pump power, the maximum output power for OCs with T = 1%, 3% and 5% were 622, 583 and 568 mW, respectively. It can be seen that for CW Tm: YLF lasers, using T = 1% OC was beneficial to obtain the maximum output power. To investigate slope efficiencies of CW lasers with different OCs, we analyzed the output power data with linear fit as shown in Fig. 4(a). The highest slope efficiency was 47.8% with T = 5% OC, which was higher than 43.9% of T = 1% and 47.2% of T = 3% OCs. Fig. 4(b) shows the AOP performance of BiQDs-SA based PQS lasers. With the absorbed pump power increased form 0.7 W–1.8 W, the AOP augment almost linearly for all three sets of T = 1%, 3% and 5%. At 1.8 W absorbed pump power, the maximum AOP of 0.33 W was obtained with T = 5% OC in PQS operation, which was higher than 0.31 W and 0.09 W for T = 1% and 3% OCs, respectively. The slope efficiencies of PQS lasers with different OCs were also obtained through linear fit. The highest slop efficiency of BiQDs-SA based Tm:YLF lasers was 28.7% for the T = 5% OC, which was higher than 8% and 26.1% for T = 1% and 3% OCs.

The absorbed pump power dependent output pulse characteristics were also summarized. From Fig. 5(a), the pulse width decreased monotonically for all OCs. In fact, the pulse width t_p can be expressed as $t_p = 8.1t_r/\ln G_0$ [30,31], where t_r is the round-trip time of light and G_0 is the small gain of the laser crystal. In our case, since we did not pump the laser crystal much hard, $\ln G_0$ can be considered as the linear increasing, leading to the almost linearly monotonical decrease of the pulse duration. Under the maximum absorbed pump power of 1.8 W, the minimum pulse width for T = 1%, 3% and 5% OCs were 499, 668 and 440 ns, respectively. Fig. 5(b) shows the variation of pulse repetition rates with the increasing absorbed pump power. It can be seen that the repetition rates show monotonically augmentation tendency for all three OCs. Within the absorbed pump power range in the laser operation, the repetition rates increased from 49 to 82, 33 to 69, and 54–94 kHz for OCs of T = 1%, 3% and 5%, respectively. The repetition rate f versus absorbed pump power can be proportional to the excited state lifetime and the pump rate [31–33]:

$$f \propto [\tau \ln(\frac{P_{ab}}{P_{ab} - P_{th}})]^{-1} \quad (3)$$

where τ is the lifetime of the excited state level in the laser crystal, P_{ab} and P_{th} represent the absorbed pump power and the absorbed pump power threshold of laser generation. It can be also concluded that the repetition rate varies almost linearly with the increasing absorbed pump power. Then the single pulse energy was calculated through dividing the average output power by the repetition rate, and the peak power was further obtained by dividing the single pulse energy by the pulse width.

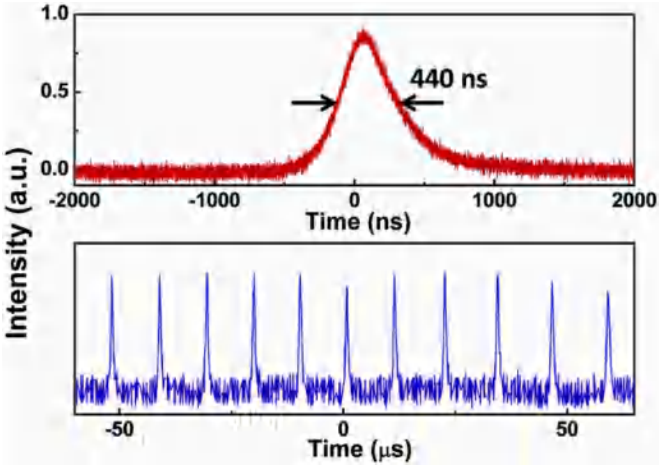

Fig. 6. Temporal profiles of pulse (top) and pulse train (bottom) with minimum pulse width.

The variations of single-pulse energies and peak powers against absorbed pump powers were also displayed in Fig. 5(c and d). Both them augmented steadily with increasing absorbed pump powers. Since the single pulse energy and peak power are calculated based on the output power, pulse width, and repetition rate, they also show a nearly linear trend with the increasing absorbed pump power. For single-pulse energy, the maximum value of 4.5 μJ was obtained with the OC of T = 3%, which was higher than that of 1.2 and 3.6 μJ for T = 1% and 5% OCs. Meanwhile, the maximum peak power of 8.1 W with the OC of T = 5% was also calculated, which was higher than that of 2.3 and 6.7 W for the cases of T = 1% and 3% OCs. From the comparisons in laser performance with the different transmittances OCs, it can be concluded that for BiQDs SA based Tm:YLF Q-switched lasers, the pulses with shortest pulse duration and highest peak power can be produced with the T = 5% OC. The temporal profile of single pulse and pulse train with the shortest pulse duration of 440 ns at the repetition rate of 94 kHz was recorded, as shown in Fig. 6.

4. Conclusions

In summary, BiQDs was successfully fabricated and employed in Q-switched Tm:YLF laser operating at 2 μm. The obtained minimum pulse width was 440 ns at a repetition rate of 94 kHz with an OC of 5% transmittance. A maximum single-pulse energy of 4.5 μJ and a maximum peak power of 8.1 W were delivered from the realized BiQDs-SA based Tm:YLF laser with OCs of T = 3% and 5%, respectively. The laser experimental results indicate the huge potentiality of BiQDs-SA acting as a new type of optical modulator in 2 μm laser generation.

Declaration of competing interest

The authors declare that they have no known competing financial interests or personal relationships that could have appeared to influence the work reported in this paper.

CRediT authorship contribution statement

Han Pan: Investigation, Methodology, Writing - original draft. **Weichun Huang:** Investigation, Resources. **Hongwei Chu:** Conceptualization, Supervision, Writing - review & editing. **Ying Li:** Formal analysis, Validation. **Shengzhi Zhao:** Formal analysis. **Guiqiu Li:** Formal analysis. **Han Zhang:** Resources, Validation. **Dechun Li:** Conceptualization, Supervision, Writing - review & editing, Funding acquisition, Project administration.

Acknowledgements

This work is supported by the National Natural Science Foundation of China (NSFC) (61575109, 21872084); Fundamental Research Fund of Shandong University (2018TB044); Natural Science Foundation of Shandong Province (ZR2018MF033).

References

[1] M.C. Gower, Industrial applications of laser micromachining, Optic Express 7 (2000) 56–67.
[2] Z. Jiao, G. He, J. Guo, B. Wang, High average power 2 μm generation using an intracavity PPMgLN optical parametric oscillator, Opt. Lett. 37 (2012) 64–66.
[3] M. Ebrahim-Zadeh, I.T. Sorokina, Mid-Infrared Coherent Sources and Applications, Springer, Barcelona, Spain, 2008.
[4] T. Bilici, H. Tabakoglu, N. Topaloglu, H. Kalaycioglu, A. Kurt, A. Sennaroglu, M. Gülsoy, Modulated and continuous-wave operations of low power thulium (Tm: YAP) laser in tissue welding, J. Biomed. Optic. 15 (2010), 038001-038009.
[5] X. Liu, K. Yang, S. Zhao, T. Li, G. Li, D. Li, X. Guo, B. Zhao, L. Zheng, L. Su, J. Xu, J. Bian, Kilo-hertz-level Q-switched laser characteristics of a Tm,Y:CaF_2 crystal, Opt. Mater. Express 7 (2017) 4352–4357.
[6] X. Liu, K. Yang, S. Zhao, T. Li, W. Qiao, Y. Yang, L. Guo, Y. Wang, H. Nie, B. Zhang, J. He, Silicon-nanoparticle-based broadband optical modulators for solid-state lasers, Opt. Lett. 43 (2018) 5957–5960.
[7] R.C. Stoneman, L. Esterowitz, Efficient, broadly tunable, laser-pumped Tm:YAG and Tm:YSGG cw lasers, Opt. Lett. 15 (1990) 486–488.
[8] X. Yang, Y. Mu, N. Zhao, Ho:SSO solid-state saturable-absorber Q-switch for pulsed Ho:YAG laser resonantly pumped by a Tm:YLF laser, Optic Laser. Technol. 107 (2017) 398–401.
[9] Q. Wang, H. Teng, Y. Zou, Z. Zhang, D. Li, R. Wang, C. Gao, J. Lin, L. Guo, Z. Wei, Graphene on SiC as a Q-switcher for a 2 μm laser, Opt. Lett. 37 (2012) 395–397.
[10] X. Zhang, H. Chu, Y. Li, S. Zhao, D. Li, Diameter-selected single-walled carbon nanotubes for the passive Q-switching operation at 2 μm, Opt. Mater. 100 (2020), 109627, https://doi.org/10.1016/j.optmat.2019.109627.
[11] L. Kong, G. Xie, P. Yuan, L. Qian, S. Wang, H. Yu, H. Zhang, Passive Q-switching and Q-switched mode-locking operations of 2 μm Tm:CLNGG laser with MoS_2 saturable absorber mirror, Photon. Res. 3 (2015) A47–A50.
[12] Z. Chu, J. Liu, Z. Guo, H. Zhang, 2 μm passively Q-switched laser based on black phosphorus, Opt. Mater. Express 6 (2016) 2374–2379.
[13] J. Qiao, S. Zhao, K. Yang, W. Song, W. Qiao, C. Wu, J. Zhao, G. Li, D. Li, T. Li, H. Liu, C.K. Lee, High-quality 2-μm Q-switched pulsed solid-state lasers using spin-coating-coreduction approach synthesized Bi_2Te_3 topological insulators, Photon. Res. 6 (2018) 314–320.
[14] K.A. Ritter, J.W. Lyding, The influence of edge structure on the electronic properties of graphene quantum dots and nanoribbons, Nat. Mater. 8 (2009) 235–242.
[15] Y. Li, Y. Hu, Y. Zhao, G. Shi, L. Deng, Y. Hou, L. Qu, An electrochemical avenue to green-luminescent graphene quantum dots as potential electron-acceptors for photovoltaics, Adv. Mater. 23 (2011) 776–780.
[16] G. Konstantatos, M. Badioli, L. Gaudreau, J. Osmond, M. Bernechea, F.P.G. de Arquer, F. Gatti, F.H.L. Koppens, Hybrid graphene-quantum dot phototransistors with ultrahigh gain, Nat. Nanotechnol. 7 (2012) 363–368.
[17] Q. Liu, B. Guo, Z. Rao, B. Zhang, J. Gong, Strong two-photon-induced fluorescence from photostable, biocompatible nitrogen-doped graphene quantum dots for cellular and deep-tissue imaging, Nano Lett. 13 (2013) 2436–2441.
[18] H.D. Ha, D.J. Han, J.S. Choi, M. Park, T.S. Seo, Dual role of blue luminescent MoS2 quantum dots in fluorescence resonance energy transfer phenomenon, Small 10 (2014) 3858–3862.
[19] Y. Xu, Z. Wang, Z. Guo, H. Huang, Q. Xiao, H. Zhang, X. Yu, Solvothermal synthesis and ultrafast photonics of black phosphorus quantum dots, Adv. Opt. Mater. 4 (2016) 1223–1229.
[20] J. Wood, S. Wells, D. Jariwala, K. Chen, E. Cho, V. Sangwan, X. Liu, L. Lauhon, T. Marks, M. Hersam, Effective passivation of exfoliated black phosphorus transistors against ambient degradation, Nano Lett. 14 (2014) 6964–6970.
[21] S. Koenig, R. Doganov, H. Schmidt, A. Neto, B. Oezyilmaz, Electric field effect in ultrathin black phosphorus, Appl. Phys. Lett. 104 (2014), 103106.
[22] A. Castellanos-Gomez, L. Vicarelli, E. Prada, J. Island, K. Narasimha-Acharya, S. Blanter, D. Groenendijk, M. Buscema, G. Steele, J. Alvarez, H. Zandbergen, J. Palacios, H.S.J. van der Zant, Isolation and characterization of few-layer black phosphorus, 2D Mater. 1 (2014), 025001.
[23] J. Pei, X. Gai, J. Yang, X. Wang, Z. Yu, D.Y. Choi, B. Luther-Davies, Y. Lu, Producing air-stable monolayers of phosphorene and their defect engineering, Nat. Commun. 7 (2016), 10450.
[24] N. Gillgren, D. Wickramaratne, Y. Shi, T. Espiritu, J. Yang, J. Hu, J. Wei, X. Liu, Z. Mao, K. Watanabe, Gate tunable quantum oscillations in air-stable and high mobility few-layer phosphorene heterostructures, 2D Mater. 2 (2014), 011001.
[25] L. Lu, X. Tang, R. Cao, L. Wu, Z. Li, G. Jing, B. Dong, S. Lu, Y. Li, Y. Xiang, J. Li, D. Fan, H. Zhang, Broadband nonlinear optical response in few-layer antimonene and antimonene quantum dots: a promising optical kerr media with enhanced stability, Adv. Opt. Mater. 5 (2017), 1700301.
[26] S. Zhang, M. Xie, F. Li, Z. Yan, Y. Li, E. Kan, W. Liu, Z. Chen, H. Zeng, Semiconducting group 15 monolayers: a broad range of band gaps and high carrier mobilities, Angew. Chem. 55 (2016) 1666–1669.
[27] M. Pumera, Z. Sofer, 2D monoelemental arsenene, antimonene, and bismuthene: beyond black phosphorus, Adv. Mater. 29 (2017), 1605299.
[28] E. Aktürk, O.Ü. Aktürk, S. Ciraci, Single and bilayer bismuthene: stability at high temperature and mechanical and electronic properties, Phys. Rev. B 94 (2016), 014115.
[29] J. Shi, H. Chu, Y. Li, X. Zhang, H. Pan, D. Li, Synthesis and nonlinear optical properties of semiconducting single-walled carbon nanotubes at 1 μm, Nanoscale 11 (2019) 7287–7292.
[30] J. Zayhowski, Passively Q-switched Nd:YAG microchip lasers and applications, J. Alloys Compd. 303/304 (2000) 393–400.
[31] H. Chu, S. Zhao, Y. Li, K. Yang, G. Li, D. Li, J. Zhao, W. Qiao, C. Feng, Simultaneous dual-wavelength operation around 1.06 μm of a LD-end-pumped, passively Q-switched Nd:GGG laser with GaAs as saturable absorber, Laser Phys. 23 (2013), 085009.
[32] K. Yang, S. Zhao, G. Li, H. Zhao, Passively Q-switching of a laser-diode end-pumped Nd:GdVO4 laser with a GaAs output coupler in a short cavity, Jpn. J. Appl. Phys. 43 (2004) 8053–8058.
[33] H. Chu, S. Zhao, K. Yang, Y. Li, D. Li, G. Li, J. Zhao, W. Qiao, X. Xu, J. Di, L. Zheng, J. Xu, Experimental and theoretical study of passively Q-switched Yb:YAG laser with GaAs saturable absorber near 1050 nm, Optic Laser. Technol. 56 (2014) 398–403.